Structure Sensitivity of Palladium Nanocrystal Catalysts in Hydrogenation of
Biomass-Derived Furanic Compounds

A Thesis
Presented to
The Academic Faculty

by

Sen Yang

In Partial Fulfillment
of the Requirements for the Degree
Master of Science in the
School of Chemical & Biomolecular Engineering

Georgia Institute of Technology
December 2015

Structure Sensitivity of Palladium Nanocrystal Catalysts in Hydrogenation of
Biomass-Derived Furanic Compounds

Approved by:

Dr. Christopher Jones, Advisor
School of Chemical &
Biomolecular Engineering
Georgia Institute of Technology

Dr. John Crittenden
School of Chemical &
Biomolecular Engineering
Georgia Institute of Technology

Dr. Younan Xia
School of Biomedical Engineering
Georgia Institute of Technology

Date Approved: October 1, 2015

To my Parents Shujie and Chunxu who made all of this possible. Their selfless support

and love is my eternal motivation.

ACKNOWLEDGEMENTS

TABLE OF CONTENTS

Page

LIST OF TABLES

LIST OF FIGURES

LIST OF SYMBOLS AND ABBREVIATIONS

5-HMF   5-Hydroxymethyl-furfural

BHF   2,5-Bis(hydroxymethyl)-furan

BHTHF   2,5-Bis(hydroxymethyl)-tetrahydrofuran

FFR   Furfural

FOH   Furfuryl alcohol

FT-IR   Fourier transform infrared spectroscopy

HMTHF   5-hydroxymethyl-tetrahydrofurfural

ICP-MS   Inductively coupled plasma mass spectrometry

TEM   Transmission electron microscopy

TGA   Thermogravimetric analysis

THFA   Tetrahydro-furfuryl alcohol

THFFR   Tetrahydro-furfural

TPR   Temperature-programmed reduction

XPS   X-ray photoelectron spectroscopy

SUMMARY

Shape-controlled palladium nanocrystals were loaded onto mesoporous silica SBA15 and studied in the hydrogenation of furfural and 5-HMF. Physio-chemical characterizations of the catalysts were conducted by nitrogen physisorption, ICP-MS, XPS, TPR, H_2 chemisorption, TEM and FT-IR spectroscopy. Catalytic tests were implemented in Parr high pressure autoclave and in liquid phase with very mild condition. By comparing the selectivity of the reaction, it was determined that the cubic palladium nanocrystals have a preference to hydrogenate the aldehyde bond in these compounds, while octahedral palladium nanocrystals prefer C=C double bond hydrogenation on furan ring. FT-IR results also support this observation.

CHAPTER 1

INTRODUCTION

1.1 Motivation

The history of human development is the history of energy upgrading. In primitive society, our ancestors used wood and grass to set fires. Back to the first and second industrial revolutions, humans used coal and petroleum to power engines. After World War 2, humans harnessed nuclear power as a new energy source. However, with a booming population and increased quality of life, energy demands are increasing dramatically. The "oil peak" is the period when the maximum rate of global petroleum extraction is reached, after which the rate of production enters terminal decline.[1] It relates to a long-term decline in the available supply of petroleum. This, combined with increasing demand, significantly increases the worldwide prices of petroleum derived products. Most significant is the availability and price of liquid fuel for transportation.[2]

The US Department of Energy indicates that "the problems associated with world oil production peaking will not be temporary, and past "energy crisis" experience will provide relatively little guidance."[3] So it is becoming extremely urgent to discover new replacement energy sources for the petroleum-based industry and, which produces both energy and chemicals.
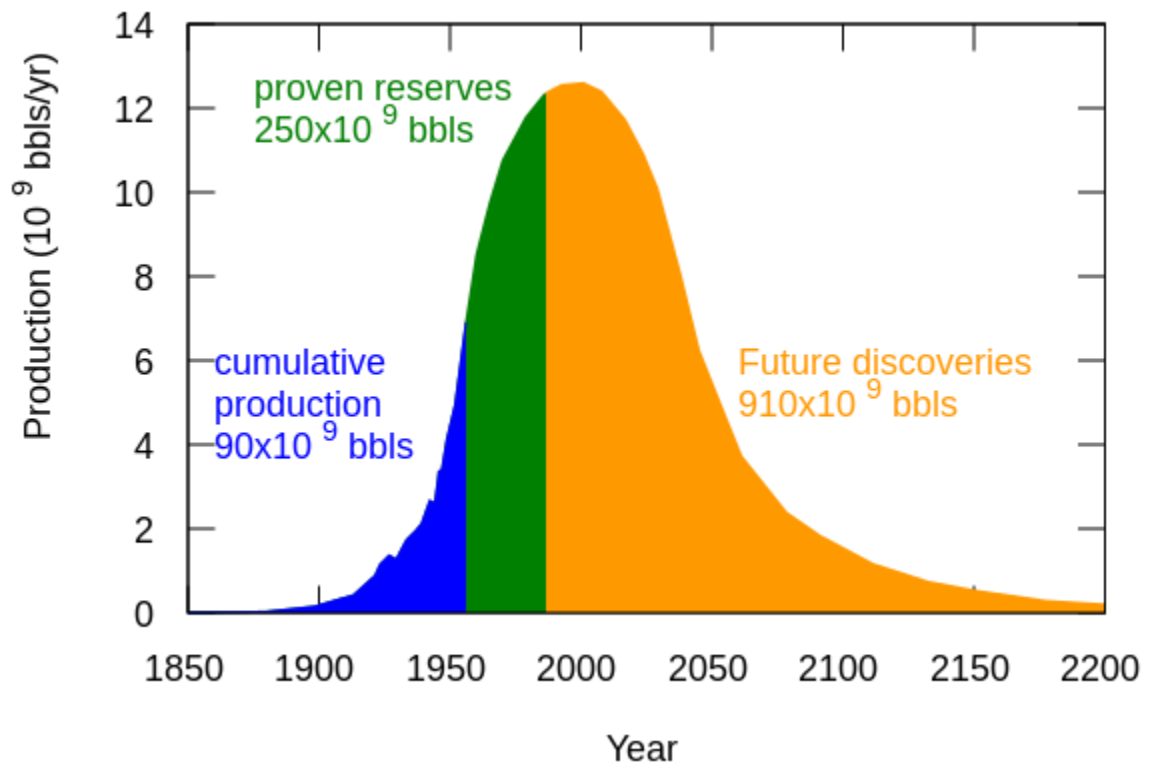
Figure 1.1 Previous and Predicted Crude Oil Production of the World[4]

People around the world are working on finding renewable energy sources and chemical feedstocks, and among all of them, biomass has drawn the most attention.[5] The production of fuel and chemicals derived from biomass, which is also known as the concept of the biorefinery, has been suggested to be a solution with high potential for alleviating the energy and feedstock shortage because of its huge amount and diversity.[6]

Renewables

biomass   hydro   wind   geothermal   solar and PV

1%

5%

9%

50%

35%
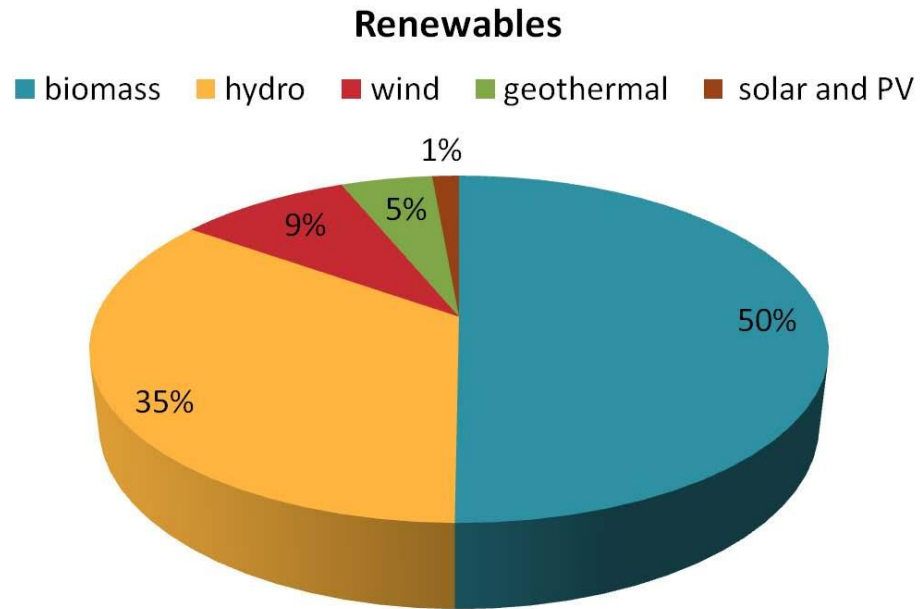
Figure 1.2 United States Total Renewable Energy Sources Production in 2012[7]
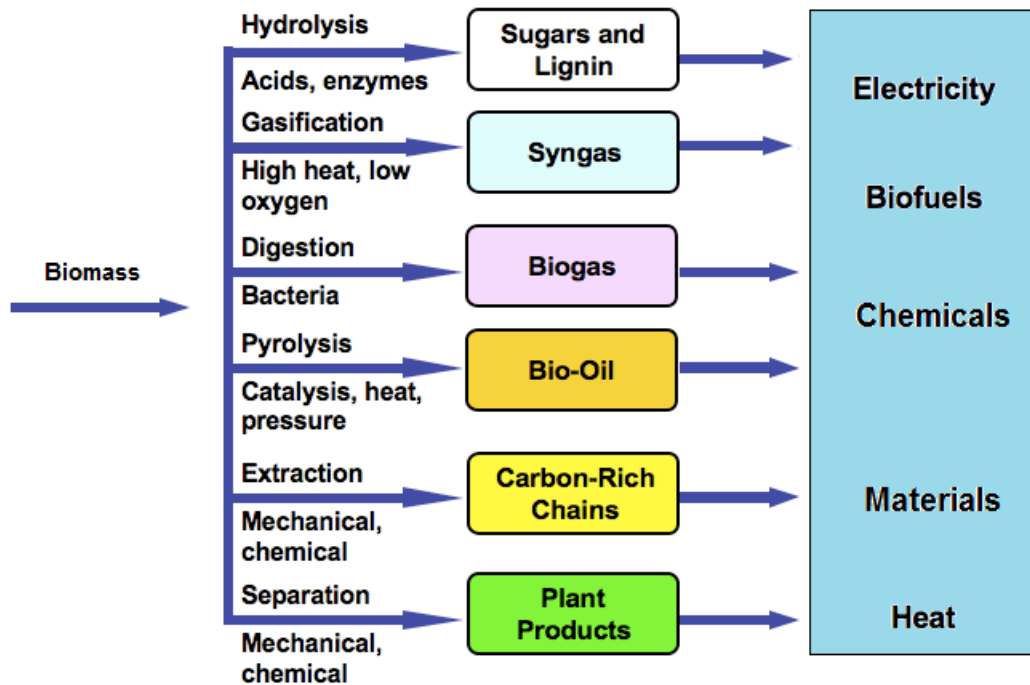
Figure 1.3 Schematic Diagram of Biomass Utilization [6, 8]

3

In recent years, the utilization of biomass, especially chemicals derived from biomass, have attracted a considerable interest.[9-12] As the urgent demand for sustainable fuels and chemicals grows, furan derivatives show huge potential to be part of the solution because of they can be easily obtained from biomass-derived carbohydrates and agricultural waste.[13, 14] A wide range of chemicals such as furfural, 5-hydroxymethyl furfural, sorbitol, levulinic acid and glucaric acid can be produced from biomass conversion and among all of them, furfural has been studied the most.[15-17] This is because furfural is considered to be a platform molecule, a key intermediate to several non-petroleum based chemicals like furfuryl alcohol (FOH), tetrahydrofurfuryl alcohol (THFA), tetrahydro-furfural (THFFR), 2-methylfuran (2-MeF), tetrahydrofuran (THF) and so on.[18-20]

1.2 Nanocrystals in catalysis

Catalysis is a well-established field with a long and illustrious history.[21, 22] Extensive knowledge is already available on how catalysis works, while enormous researches are being conducted to develop better catalysts as well.[23-25] Nevertheless, much still remains to be done in this field. New advances in nanotechnology offer promise to provide tools to expand frontier.

Because catalytic metals are sometimes expensive, people tend to disperse small nanoparticles onto high surface area supports. This optimizes their surface-to-bulk ratio (it is the surface that promotes catalysis) and also offers the opportunity to create new

synergies at the interface of the support for new functionalities.[26] However, in the past, there have been limited number of approaches to prepare these dispersed catalysts, and they have offered limited control, if any, on the nature of the final nanoparticles produced. Typically, a distribution of particles is obtained with a variety of sizes and shapes. In many instances, different facets of a solid display different catalytic behavior. [27, 28] It would be highly desirable to have full control of the design and production of specific catalytic sites with specific local geometries.

This synergy between basic mechanism research in catalysis and new synthetic nanotechnologies promises to take the field of catalysis into new, unexplored areas, which may allow the development of selective processes for the catalytic synthesis of complex molecules. The ability to control the shape of nanoparticles in particular is likely to provide a handle on the tuning of so-called structure-sensitive catalytic reactions.[29, 30] With the help of that, we can answer questions like how new selective catalysts based on shape-defined nanoparticles can be designed to understand the reaction of interest.

Lim et al. has successfully synthesized shape-controlled Pd nanocrystals.[31] Crespo-Quesada et al. recently applied shape-controlled nanocrystals in acetylene hydrogenation, showing that (111) surfaces in Pd octahedrons were more active than the (100) faces in Pd cubes.[32] Jin et.al developed additional structures of Pd nanocrystals and discussed their catalytic application.[33] Xia et al. recently reported the successful synthesis of Ir coated Pd nanoparticles, which shows the potential for synthesizing other nanocrystals by coating methods. In furfural hydrogenation, Pt nanoparticles have been applied to probe

structure sensitivity during vapor phase furfural hydrogenation.[34] Their results show cubic Pt nanoparticles yield equal amounts of furan and furfuryl alcohol, while octahedral nanoparticles yield mostly furfuryl alcohol. However, tuning of the structure of the Pd nanocrystals as a way to tune the selectivity in liquid phase furan conversions has not been reported.

1.3 Previous work on furfural & 5-HMF hydrogenation

As relatively oxidized molecules compared to most petroleum-derived products, the hydrogenation or hydrodeoxygenation of furfural and HMF has been widely studied.[35-39] Hydrogenation of furfural and 5-HMF has been explored over various metal catalysts (e.g. Ni, Co, Cu, Ru Pt, Pd, Ir) in the six decades since Wojcik reported the hydrogenation of furanic compounds using Raney nickel and Cu-Cr in 1948.[40] Pd catalysts are among the well-studied metals, showing potential to convert furfural and HMF into a variety of products by changing the reaction conditions. Hronec et al. have reported that furfural was primarily converted into THFA using a Pd/C catalyst at a temperature of 160 °C and pressure of 80 bar H_2.[41] Meanwhile, Nakagawa et al. reported that lower temperatures (2 °C) can be used to convert furfural mostly into FOH, with the presence of THFFR as a side product.[42] Pd can also hydrogenate furfural into 2-MeF in the presence of an acid co-catalyst.[43]

Table 1.1 Representative works from the literature in the hydrogenation of furfural

No.	Catalyst	Reaction condition	Conv. %	Y_{FA} %	Ref.
1	5% Pt/C	175 ℃, 80 bar H_2, 0.5 h, n-butanol solvent	99	48	[41]
2	5% Pd/Al$_2$(SiO$_3$)$_3$	150 ℃, 20 bar H_2, 4 h, acetic acid-assisted	57	30	[43]
3	2% Ir/TiO$_2$	90 ℃, 6.2 bar H_2, n-heptane/ethanol	30	30	[44]
4	2% Ir-ReOx/SiO$_2$	30 ℃, 8 bar H_2, 6 h, water solvent	>99	>99	[45]
5	Co-Mo-B alloy	100 ℃, 10 bar H_2, 3 h, ethanol solvent	>99	>99	[46]
6	Ni-Ce-B alloy	80 ℃, 10 bar H_2, 3h, ethanol solvent	97	~97	[47]
7	2% Ru/C	165 ℃, 25 bar H_2, MTHF solvent	91	42	[48]
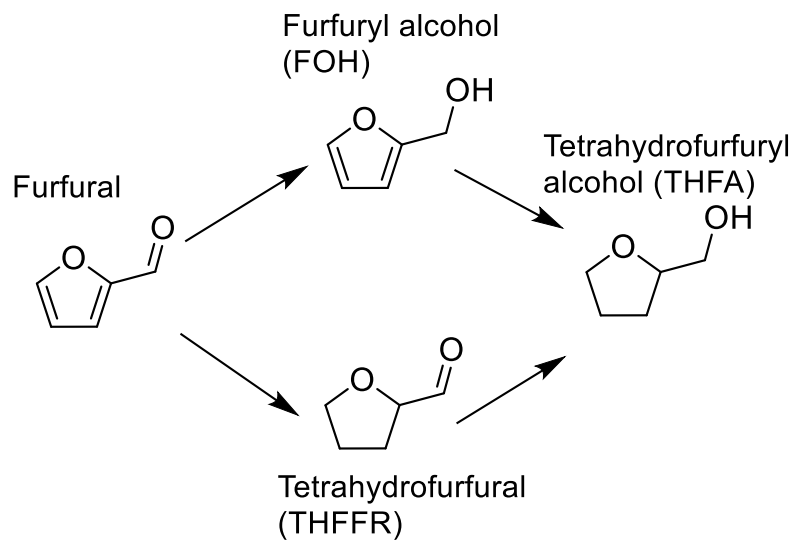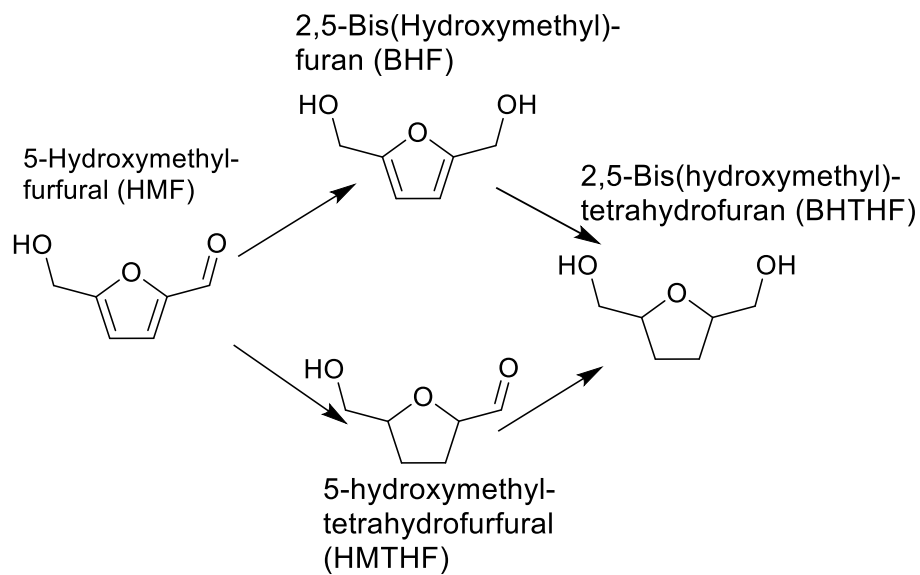
Figure 1.4 Reaction pathways for hydrogenation of furfural (a) and HMF (b)

Figure 1.4 illustrates the typical reaction pathways during the hydrogenation of furfural

and HMF. The two types of unsaturated bonds in furfural (carbonyl and olefin) give the

possibility of two primary reaction pathways. In the top pathway shown in figure 1, the

carbonyl species in furfural is first reduced, producing furfuryl alcohol (FOH), with a

secondary hydrogenation leading to the saturated product tetrahydrofurfuryl alcohol

(THFA). In the bottom pathway, the olefin species are first reduced to yield

tetrahydrofurfural (THFFR), followed by continued reduction to produce THFA.

1.4 Objective

In this study, shape-controlled Pd nanocrystals supported on SiO_2 (SBA15) are applied as

catalysts to investigate the structure sensitivity of furfural and 5-HMF hydrogenation.

Liquid phase reactions under mild reaction conditions were adopted to monitor the

generation of THFFR and HMTHF. In addition, a polycrystalline Pd catalyst was also

used to compare the selectivity differences with the well-defined catalysts. By comparing

the product and selectivity at same reaction times under identical reaction conditions, the

structure selectivity of the hydrogenation of furfural and 5-HMF on Pd surfaces has been

explored.

CHAPTER 2

EXPERIMENTAL DESIGN

2.1 Catalytic material synthesis

Chemicals and gases

The following chemical were purchased from Sigma-Aldrich and used without further purification: furfural (99% purity), HMF (≥99% purity, FG), sodium tetrachloropalladate (≥99.99% purity, trace metals basis), poly(vinylpyrrolidone) (MW~55,000), L-ascorbic acid (≥99% purity, reagent grade), potassium bromide (≥99% purity, reagent grade), potassium chloride (≥99% purity, reagent grade), citric acid (≥99% purity, reagent grade), Pluronic P123 (average Mn~5800), tetraethyl orthosilicate (98% purity, reagent grade). Hydrogen, helium, nitrogen and air were purchased from Airgas USA.

Shape-controlled Pd nanocrystals

Palladium nanoparticles were synthesized separately from the silica support. For cubes, poly(vinylpyrrolidone) (PVP, 105 mg), L-ascorbic acid (60mg), potassium bromide (KBr, 5 mg) and potassium chloride (KCl, 185 mg) were dissolved into 8 mL of water. Sodium tetrachloropalladate (Na_2PdCl_4, 19 mg/mL water solution) 3 mL was then added dropwise and heated at 80 °C for 3 h. After reaction, the sample was washed by water twice and ethanol once in an ultracentrifuge at 55,000 rpm. For octahedrons, L-ascorbic acid was replaced by citric acid (180 mg) and KBr and KCl were omitted. Finally, the nanoparticles were dispersed into 5 mL of ethanol.

SBA15

For a typical batch of SBA15, the copolymer template (Pluronic P123®, 48g) was dissolved in hydrochloric acid (HCl, 240 mL) and water (1272 g). Then tetraethyl orthosilicate (TEOS, 92.52 g) was added and vigorously stirred at 40 °C for 20 h. After dissolving and mixing, the white sediments were separated by vacuum filtration and washed with DI water several times to remove residual copolymer. The while solid was then aged in oven at 150 °C for 24 h, then calcined at 550 °C for 12 h in air.

Pd Loading onto silica

SBA15 powder was dispersed in 50 mL of ethanol, and then the nanocrystal suspension was added dropwise under sonication. The mixture was subsequently sonicated for 3 h. The black sediments were then washed by water 3 times during centrifugation, and finally, the sediments were separated by centrifuge and dried at 80 °C overnight in air.

Polycrystalline Pd nanocrystal catalyst

An incipient-wetness impregnation method was applied to prepare a polycrystalline silica-supported Pd catalyst. Palladium nitrate [$Pd(NO_3)_2$ 0.11g] was dissolved in water of the same volume (1.06 mL) as the pore volume of 0.96g of SBA-15. The Pd solution was added to SBA15 dropwise with vigorous stirring for 30 min followed by subsequent drying at 80 °C for 12 h in air. The mixture was then placed in ceramic crucibles and calcined at 500 °C for 3 h in air. Before use in catalytic reactions, the catalyst was reduced by H_2 at 100 °C in the same reactor used for catalytic tests to reduce polycrystalline Pd nanoparticles.

11

2.2 Catalyst characterization

Inductively coupled plasma mass spectrometry (ICP-MS)

The elemental molar composition of the catalysts was measured by ICP-MS
(PerkinElmer Elan DRC II ICP-MS). Typically, 0.007 g sample was dispersed into 5 mL
of ethanol. Then, 0.1 mL of the suspension was taken into 1 mL aqua regia and 8.9 mL of
nitric acid (HNO_3, 1%wt). The mixture was stirred for 24 h to ensure the complete
dissolution. The final samples were diluted with 30 mL of 1%wt HNO_3 and analyzed by
the mass spectrometer.

Temperature-programmed reduction (TPR)

H_2-temperature programmed reduction (H_2-TPR) was conducted using a Micromeritics
AutoChem II 2920 chemisorption instrument. For a typical experiment, 50 mg sample
was placed in a quartz tube and heated to 80 ℃ for 1 h under helium to remove
impurities. The sample was next cooled to room temperature under flowing helium, and
then TPR was carried out using a 10% H_2/Ar (V/V) mixture with 20 cm^3/min flow rate.
The temperature ramp was 5 ℃/min to 300 ℃, and the reduction was followed with a
thermal conductivity detector.

Thermogravimetric analysis (TGA)

Thermogravimetric analysis (TGA) was carried out by using Netzsch STA 409 TGA-
DSC. About 30 mg sample was loaded in a pan. Then it was heated from 20 ℃ to 900 ℃
with a rate of 10 ℃ /min in air with flow rate of 90 mL/min.

Nitrogen physisorption

N_2 adsorption–desorption isotherms were measured by Tristar II 3020 apparatus from Micromeritics. Samples were first degassed at 110 ℃ under vacuum for 12 h prior to the measurements. The specific surface area (by the BET method) and pore volume (by T-plot method) were obtained by the software of the apparatus.

H_2 chemisorption

H_2 chemisorption was conducted with a Micromeritics AutoChem II 2920 chemisorption instrument. For a typical run, 50 mg sample was placed in a quartz tube and heated to 300 ℃ under H_2 flow (25 cm^3/min) to thoroughly reduce the sample. After reduction, the sample was cooled to room temperature under 25 cm^3/min He flow. Then approximately 20 pulses of 10% H_2/Ar were applied to the sample and the uptake was recorded via the TCD signal. The results were analyzed by software associated with the equipment.

X-ray photoelectron spectroscopy

XPS analysis was complemented using Thermo K-Alpha spectrometer employing a monochromatic Al K X-ray source. Pressures near 5×10^{-8} Torr were observed in the analytical chamber during surface analysis. The binding energies (BE) of all the elements were referenced to the C 1s peak of contaminant carbon at 284.6 eV with an uncertainty of ±0.2 eV.

Transmission electron microscopy

TEM images were obtained using Hitachi-HT7700 microscope operated at 120 kV. For a typical sample, the catalyst powder was dispersed in ethanol and then dropped on carbon-coated copper grids.

FT-IR spectroscopy

Fourier transform infrared (FT-IR) spectroscopy experiments were performed using a Varian 640 infrared spectrometer equipped with an internal reflection element made of diamond (angle of incidence 45 °, three active reflections). Before the measurements, the crystal surface was washed using ethanol to remove possible contaminants. The sample for analysis (about 10 μL of colloidal solution containing the nanoparticles in ethanol) was drop-cast on the top of the crystal and dried. IR spectra were recorded in the range of 4000 ~ 400 cm^{-1} with a resolution of 1 cm^{-1}, using a cooled, deuterated and L-alanine-doped triglycine sulfate (DLaTGS) detector.

2.3 High pressure batch reactor

Experiments were performed in a 300 mL stainless steel Parr autoclave. A four bladed pitch turbine impeller was used to agitate the liquid phase. A calculated quantity of catalyst was first directly put in [Pd(Cube), Pd(Octa)] or reduced in hydrogen at 100 ℃ for 1 h before use [Pd(PC)]. Calculated quantities of furfural and water were then charged into the autoclave. The reactor was purged with hydrogen 5 times to remove air, followed by further pressurization with hydrogen to 200 psig. Cooling water were both applied to

maintain a constant temperature (20 ℃) by a U-shape coil inside the reactor. An initial

sample was collected when the temperature in the autoclave reached the desired value

and 1 mL of sample was collected at an interval of 15 min over the first hour of reaction,

followed by sampling every 30 min over the following two hours. A constant hydrogen

pressure was maintained throughout the reaction. A typical reaction was carried out with

furfural (4.8 g, 0.05 mol), water (90 g, 5 mol), catalyst (0.5 g) at 20 ℃, 200 psig of

hydrogen at an agitation speed of 500 rpm.

Figure 2.1 Parr pressure autoclave system setup

Figure 2.2 Varian CP3800 GC system

2.4 Methods of reaction analysis

The samples were analyzed by a gas chromatograph system (Varian CP3800) with flame ionizing detector (FID). The polyethylene-glycol-based capillary column (Rtx-Wax Cap column 30m-0.25mm- 0.25um) was applied. The oven temperature was programmed to begin at 50 ℃ for 5 min and ramped to 150 ℃ at 10 ℃/min with a hold time of 2 min. Before injection, every sample was weighted then the measured quantity of 1,4-dioxane, as an external standard, was added into sample vial and mixed abundantly. Next, 0.5 microliter of sample was injected with a split ratio of 150:1 into the GC. Helium was used as carrier gas at a flow rate of 3.0 cm^3/min. Conversion and selectivity were calculated as shown below.

$$Conversion = \frac{initial\ moles\ of\ FFR - final\ moles\ of\ FFR}{initial\ moles\ of\ FFR} \times 100\% \tag{1}$$

$$Selectivity = \frac{moles\ of\ desired\ product\ formed}{initial\ moles\ of\ FFR} \times 100\% \tag{2}$$

CHAPTER 3

RESULTS AND DISCUSSION

3.1 Transmission Electron Microscopy (TEM)

Figures 3.1 and 3.2 give TEM images of different Pd nanoparticle samples and statistics measured from the images. Image a) and b) are unsupported nanoparticles immediately after synthesis. The size and shape of the cubes and octahedrons are very uniform, while the structural differences between two types can be clearly seen. Images c) and d) are images of the nanoparticles loaded on SBA15. The particles are mostly on the external surface of the SBA15 and the nanoparticle structures remain unchanged, indicating the loading process did not compromise the nanocrystal quality. The size of the nanocrystals obtained from TEM statistics match well the results from H_2 chemisorption (see below). Images e) and f) are from the catalysts after using in catalytic reactions. The shapes were still unchanged, indicating that the reaction did not destroy the structure either. Image g) is the SBA15 supported polycrystalline nanoparticle sample. There are many dark dots with various shapes on this material, which are the palladium nanocrystals. Image h) is the bare mesoporous silica SBA15, where the parallel mesoporous can be clearly seen.
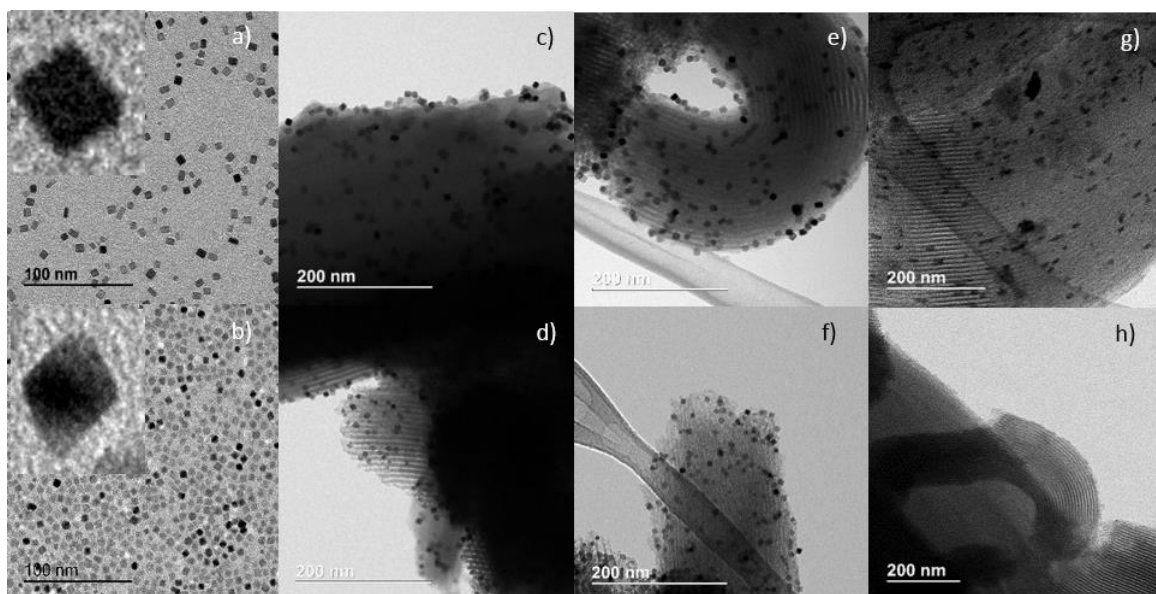
Figure 3.1 TEM images of a) unsupported Pd cubes and b) octahedrons, top left are

zoomed in single particles, c) Pd(Cube) fresh, d) Pd(Octa) fresh, e) Pd(Cube) used,

f) Pd(Octa) used, g) Pd(PC) fresh and h) SBA15
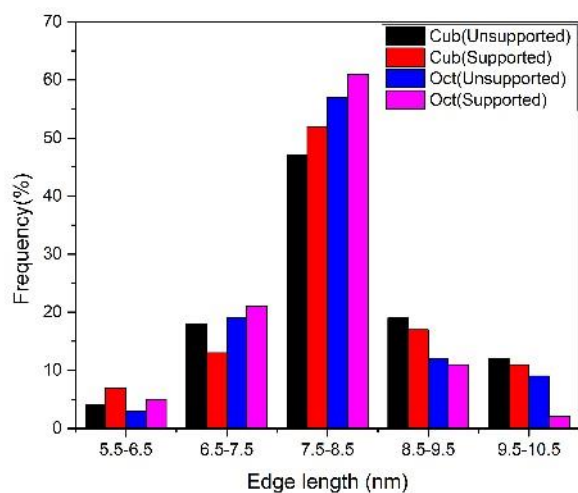
Figure 3.2 TEM statistics describing Pd particle sizes of the various catalysts

3.2 Temperature Programmed Reduction (TPR)

Figure 3.3 shows the TPR profiles of fresh samples of the three catalysts. One peak is observed in each profile in the range of 50-100 ℃. This is due to hydrogen consumption associated with the reduction of oxidized surface palladium to metallic palladium. The peak for the Pd(PC) sample is dramatically larger than the peaks for the other two catalysts, which suggests that much of the palladium in fresh Pd(PC) are in an oxidized state, while the shape-controlled nanocrystals were mostly in the metallic state prior to TPR. By integrating the TPR profile, the cumulative H_2 consumption of Pd(Cube) is 12.4 μmol and that for Pd(Octa) is 11.7 μmol, both much lower than the amount of H_2 needed for thoroughly reducing the fully oxidized Pd nanocrystal surface.) Given that all the catalysts have a similar metal loading based on elemental analysis, these differences demonstrate the significantly higher degree of oxidation of the polycrystalline catalyst. The TPR profile of the polycrystalline catalyst ends at 100 ℃, indicating the Pd(PC) is fully reduced at this moderate temperature. Both the Pd(Cube) and Pd(Octa) catalysts are fully reduced by a temperature of 130 ℃.
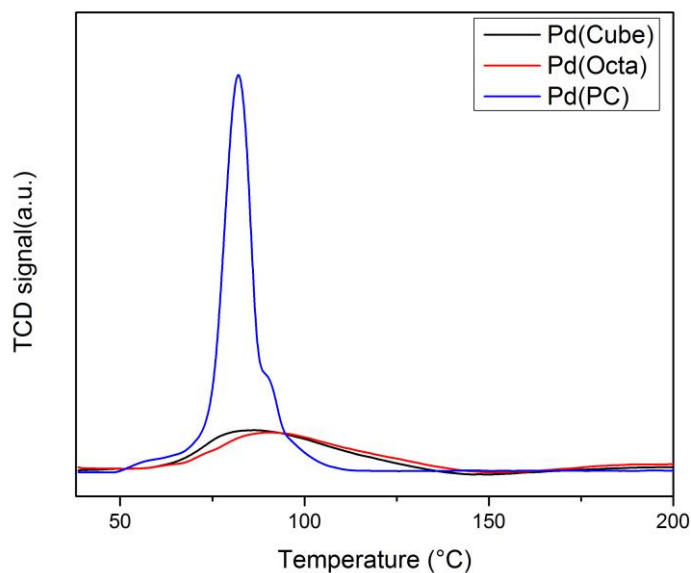
Figure 3.3 TPR profiles of the three catalysts, Pd(Cube), Pd(Octa) and Pd(PC)

3.3 Elemental analysis

The elemental analysis results are shown in Table 2. The ICP-MS results give the bulk

palladium loading while XPS results represent the external surface. The results of ICP-

MS are very close to each other, which means the metal loadings of all the catalysts are

similar. Meanwhile, the Pd(Cube) and Pd(Octa) samples show much higher external

surface Pd concentrations than Pd(PC) because the different metal loading methods. For

Pd(Cube) and Pd(Octa), the large (relative to the pore size) nanoparticle were loaded by

sonication. The nanocrystals will stay primarily on the surface of SBA15 because it is

larger than the pores on SBA15, showed in nitrogen physisorption. In contrast, the Pd(PC)

catalyst loaded by incipient wetness of a molecular Pd precursor. This method will

adsorb Pd salt solution into the pores of SBA15 and after calcination, the Pd species are

21

dispersed and stabilized in an oxidized state. This result can be also justified by the TEM images discussed above. Trace amount of N was found in the XPS result as well. It is because PVP is used as a stabilizer when synthesizing shape-controlled nanocrystals and very little PVP left on nanocrystal surface. The amount of PVP residue are quite similar for Pd(Cube) and Pd(Octa), which can also be validated by TGA results. Also, no PVP residue was found in Pd(PC).

Table 3.1 Elemental analysis results of bulk (ICP-MS) and surface (XPS) compositions

Catalysts	ICP-MS Pd wt%	ICP-MS Pd/Si mole ratio	XPS Pd/Si mole ratio	XPS N/Si mole ratio
Pd(Cube)	1.74	0.01	0.05	0.01
Pd(Octa)	1.65	0.01	0.04	0.01
Pd(PC)	1.48	0.01	0.01	-

3.4 Thermogravimetric analysis (TGA)
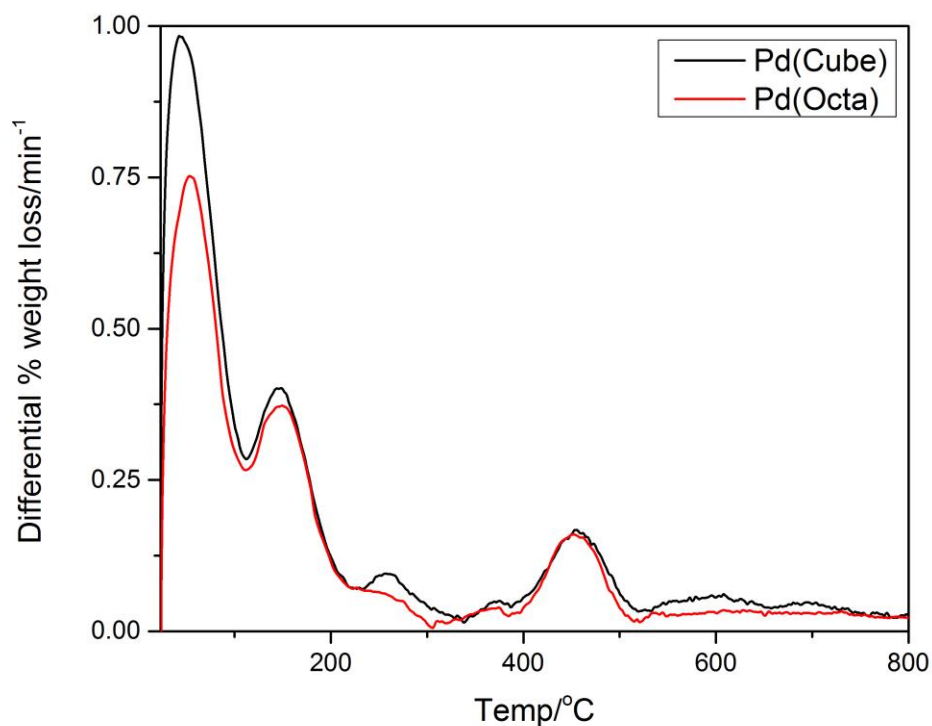
Figure 3.4 Differential percentage weight loss of Pd(Cube) and Pd(Octa)

Thermogravimetric analysis results are displayed in Figure 3.4. The peaks before 100 °C belong to sample water bake-off. Peaks between 100 °C and 200 °C belong to silanol group dehydration.[49] Peaks after 400 °C belong to PVP decomposition.[50] The PVP decomposition peak of both Pd(Cube) and Pd(Octa) are very similar, which indicates that the PVP residues on two shape-controlled nanocrystals are very close to each other. This result matches the XPS results as well.

3.5 H₂ Chemisorption

Table 3.2 gives the results of H_2 chemisorption. Metal dispersions using these data are calculated by equation 3, below. The turnover frequency (TOF) is calculated using initial rates by equation 4. Crystal sizes obtained from chemisorption analysis are similar to those derived from TEM. The metal dispersion of Pd(PC) is slightly better due to the presence of some very small nanoparticles, while the Pd(Cube) and Pd(Octa) are quite similar. Overall, all three can be considered to be very close in dispersion, making their comparison useful and meaningful. The active metal surface area and cumulative H_2 uptake of the Pd(Cube) and Pd(Octa) samples are larger than Pd(PC), which because the nanocrystals loaded on the SBA15 surface have better metal dispersion. Combining chemisorption data and reaction data, the TOF values were calculated.

Dispersion:

$$\%M_{Disp} = \frac{1}{22414} \times \frac{V_T \times SF_{CALC}}{\omega_{Pd}/W_{A,Pd}} \tag{3}$$

where $\%M_{Disp}$ is metal dispersion, V_T is volume intercept derived from the volume differences between the selected points of the first analysis and repeating analysis (cm^3/g STP), and SF_{CALC} is the calculated stoichiometry factor.

Turnover frequency:

$$TOF = \frac{Product\ Molecules}{Active\ sites \times Time} \tag{4}$$

Table 3.2 H$_2$ chemisorption and turnover frequency result

Catalysts	Crystal size (nm)	Active metal surface (m^2/g sample)	Metal dispersion	Cumulative H$_2$ quantity (10^{-6} mol)	TOF in FFR reaction (h^{-1})
Pd(Cube)	8.4	1.5	14%	31	173
Pd(Octa)	7.7	1.6	16%	34	162
Pd(PC)	7.7	1.1	11%	23	260

3.6 BET Surface area

The BET surface areas and BJH pore diameter of the three catalysts, (i) palladium

nanocubes [Pd(Cube)]on SBA15, (ii) nanooctahedra palladium [Pd(Octa)] on SBA15,

and (iii) polycryctalline palladium [Pd(PC)] loaded on SBA15, alongside the bare support,

are listed in Table 3.3. The BET surface areas of the loaded nanocrystal samples are very

similar overall around 795-835 m^2/g, while fresh SBA15 has a little higher SA. This

result suggests that the loading process will compromise some SA, however, it is not a

dramatic change. The SBA15 still holds its structure, which could also be observed by

TEM. The pore diameter of SBA15, comparing to the TEM statistics of nanocrystals, is

smaller. This explained why the nanocrystals will stay on the surface of SBA15, rather

than into the pore.

Table 3.3 BET surface area of various catalysts

Catalysts	BET(m^2/g)	BJH pore diameter (nm)
Pd[Cube]/SBA15	825	6.6
Pd[Octa]/SBA15	832	6.7
Pd[PC]/SBA15	795	6.1
SBA15	907	6.8

3.7 Catalytic tests

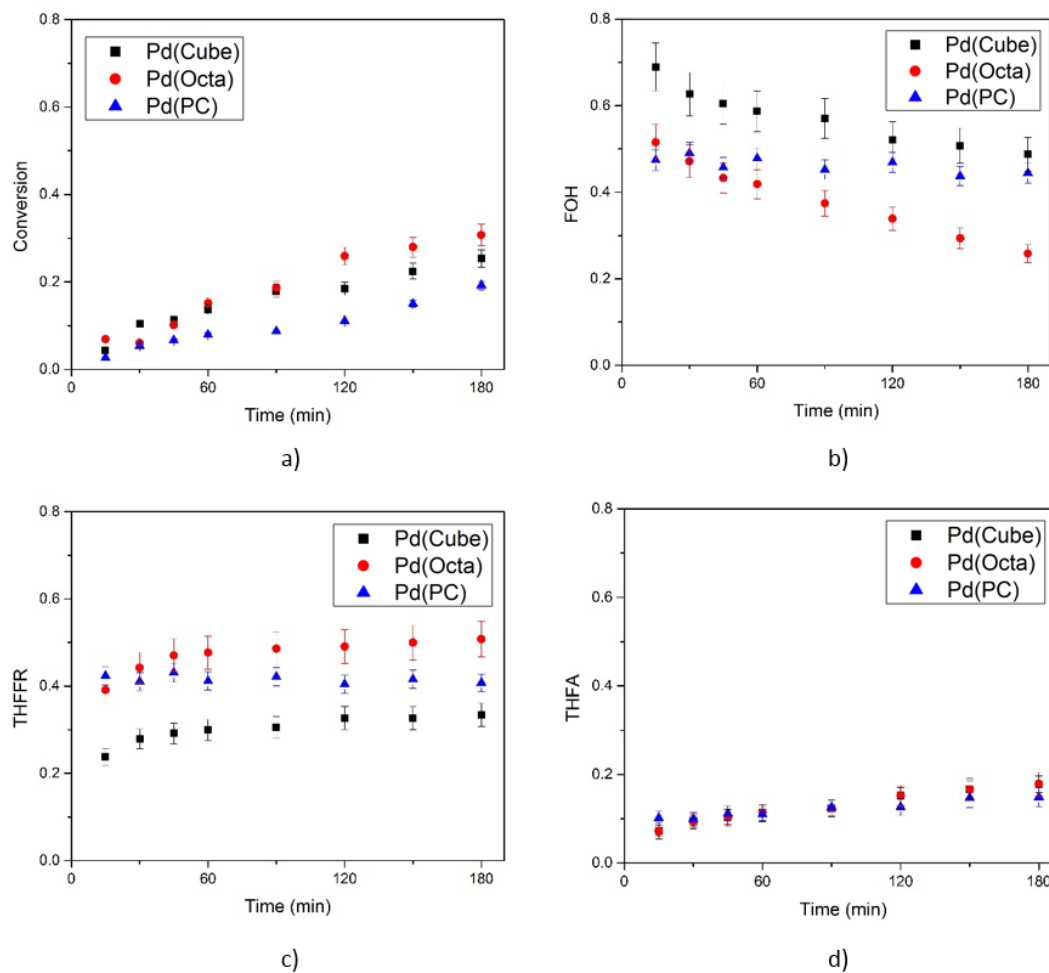*Furfural hydrogenation*

Figure 3.5 Furfural hydrogenation results: a) Conversion, b) Selectivity of furfuryl alcohol (FOH), c) Selectivity of tetrahydrofurfural (THFFR), d) Selectivity of tetrahydrofurfuryl alcohol (THFA)

Catalytic test results of the hydrogenation of furfural are shown in Figure 3.5. The conversions of the Pd(Cube), Pd(Octa) and Pd(PC) catalysts are very close, which might

indicate that the reaction rates of furfural hydrogenation are not very structure sensitive. The selectivity for THFA of all the three catalysts are quite low and similar, which is because in the first 3 hours of reaction time, THFA is not the main product. The production of THFA comes from hydrogenation of FOH and THFFR. When in mild reaction conditions, the first step reactions are dominating and leave few open active sites for the second step reaction in the series. But when the reaction time is extended, the intermediates will finally become converted to THFA.

The selectivity of THFFR for the three catalysts are somewhat different, with Pd(Cube) ~30%, Pd(PC)~ 40% and Pd(Octa) ~50%. We found this difference in all the duplicate tests and generated error bars, as displayed in the figure. This phenomena might be associated with differences in the adsorption preference of furfural on the Pd nanocrystal surfaces. For the Pd(Cube) sample , the surface crystal planes are dominated by Pd(100), while for the Pd(Octa) material the surface is covered by more Pd(111).[31] The Pd(PC) could be considered as a mixture of both. When adsorbing furfural on its active sites, the Pd(Cube) might prefer to adsorb the C=O double bond of aldehyde, and convert it into an alcohol. However, the reaction data suggest that Pd(Octa) may prefer to adsorb the C=C double bond on the furan rings. Which can then be hydrogenated into saturated groups. The main absorbed bond will be first hydrogenated and thus, it is hypothesized that the difference in adsorption gives the different observed products over the different crystal faces. This will be discussed further, below.

5-HMF hydrogenation

To justify this hypothesis, we conducted 5-HMF hydrogenation tests as a comparison and the results are shown in Figure 3.6. The conversion during 5-HMF hydrogenation is higher than for furfural due to the higher activity of the 5-HMF molecule.[42] The selectivity of HMTHF still shows the differences observed above among the three catalysts, Pd(Cube) ~40%, Pd(PC) ~30% and Pd(Octa) ~20%. The selectivity of HMTHF in 5-HMF hydrogenation are lower than the selectivity of THFFR in furfural hydrogenation because on the 5-HMF molecule, there is one more hydroxyl on the furan ring. This hydroxyl makes the adsorption of the C=C double bond on the furan ring more difficult. At the same time, the selectivity of HMTHF of Pd(Cube) is still higher than that of Pd(Octa), which is consistent with the hypothesis above about preferential adsorption on different surfaces.
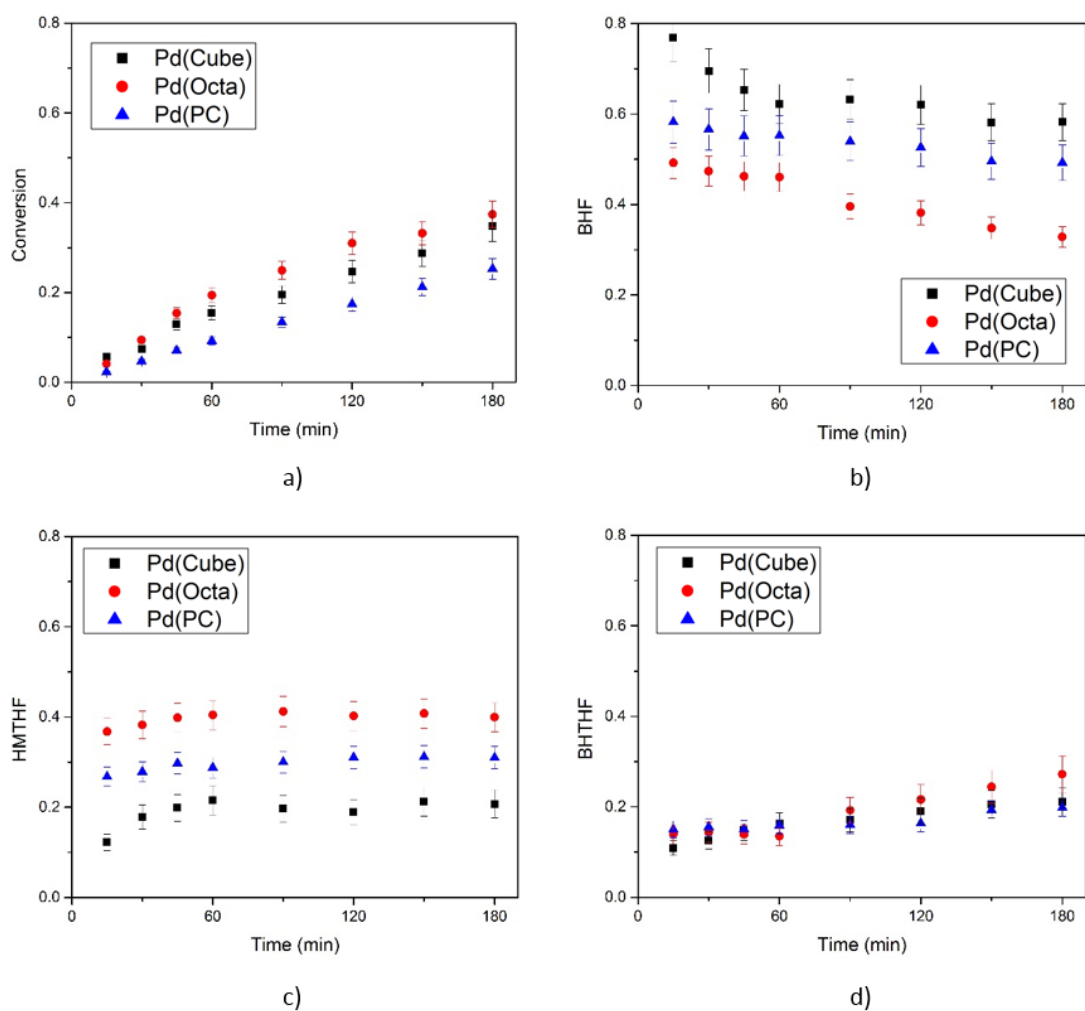
Figure 3.6 5-HMF hydrogenation results: a) Conversion and b) Selectivity of 2,5-Bis(hydroxymethyl)-furan (BHF), c) Selectivity of 5-hydroxymethyl-tetrahydrofurfural (HMTHF), d) Selectivity of 2,5-Bis(hydroxymethyl)-tetrahydrofuran (BHTHF)

3.8 FT-IR study of furfural adsorption

To further probe the preferential adsorption hypothesis, we conducted an FT-IR

investigation using unsupported Pd nanoparticles. The results are shown in Figure 3.7.

The samples *Cube* and *Octa* are unsupported nanoparticles in ethanol that have been

stirring for 3 hours and *Cube+FOH* and *Octa+FOH* are unsupported nanoparticles with

5%wt furfuryl alcohol in ethanol that have been stirring for 3 hours. The suspension then

was separated by centrifuge and the samples were washed by ethanol 3 times to remove

unabsorbed furfuryl alcohol, and finally re-disperse the nanocrystals in ethanol. After

dropping the suspension on the sample-holder of FT-IR equipment, we let the sample dry

in air for 15 min to evaporate the residual ethanol. The peak at 1200 cm^{-1} indicates the C-

H bond stretch, which comes from the PVP residue on the nanocrystal surface[50] and

the 1050 cm^{-1} band is the C-O stretch, which usually indicates the presence of an alcohol,

in this case, furfuryl alcohol. By normalizing the C-H peak, which is because the similar

PVP residue amount on two kinds of shape-controlled nanocrystals based on TGA and

XPS results, we compared the intensity of the C-O peak to compare the adsorbed furfuryl

alcohol amount. There are almost no peaks in the profile of *Cube* and *Octa*. However,

peaks are present in the *Cube+FOH* and *Octa+FOH* spectra. The C-O stretch in

Octa+FOH is much higher than that of *Cube+FOH*, which might imply that the

octahedral palladium nanocrystals adsorb furfuryl alcohol more effectively than the cubic

ones. Because there is only one kind of unsaturated bond, the C=C double bond on the

furan ring existing in the furfuryl alcohol molecule, the result shows the preference of the

octahedral crystals in adsorbing the C=C double bond on the furan ring. Taking into

further, the octahedral crystals will preferentially adsorbs and hydrogenates the furan
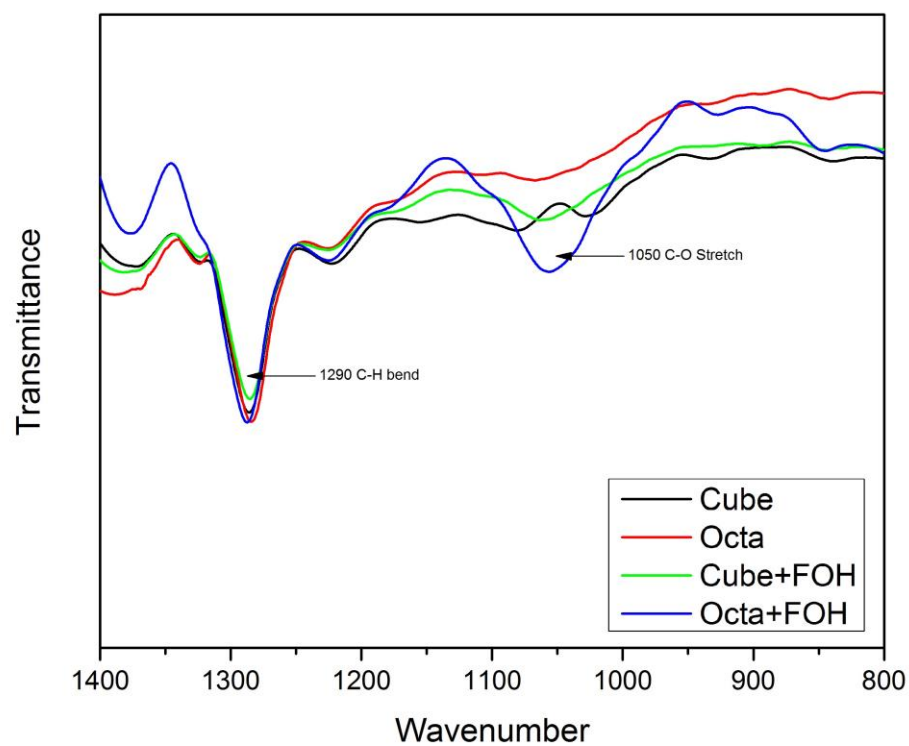
unsaturated bonds

Figure 3.7 FT-IR spectra of unsupported Pd nanocrystals with and without exposure to

furfuryl alcohol

CHAPTER 4

CONCLUSIONS AND SUGGESTION FOR FUTURE WORK

In the present work, the catalyst structure sensitivity of furfural and 5-HMF

hydrogenation have been discussed. With the help of shape-controlled palladium

nanocrystals, the catalytic results of nanoparticle catalysts of different shapes with similar

size, metal loading and active metal surface area were compared. For cubic palladium

nanocrystals with surface crystal planes of primarily Pd(100), the aldehyde C=O bonds

were suggested to be preferentially adsorbed and reacted. For octahedral palladium

nanocrystals with surface crystal planes of primarily Pd(111), the unsaturated C=C bonds

on the furan ring were suggested to be preferentially adsorbed and reacted. (Figure 4.1)

The results of catalytic tests and FT-IR spectra support this hypothesis. However, the

differences in selectivity are modest, and future work using shaped nanoparticles of

different metals might be suggested to offer greater differences.
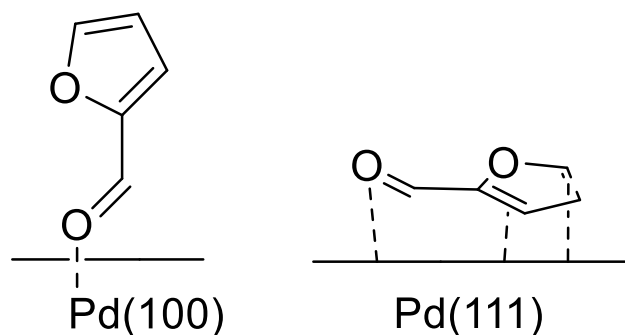
Figure 4.1 Adsorption preference on Pd surface

In addition to this research, vapor phase hydrogenation of furfural and 5-HMF can also

be applied using these shape-controlled nanoparticles to probe high temperature Pd

adsorption structure sensitivity. Also, other palladium catalyzed reactions like the crotonaldehyde can also be applied using shape-controlled Pd nanoparticles to probe facet-influenced selectivity. Recently, Xia et al. published a paper on coating iridium on the surface of palladium nanoparticle surface, which will expose exact the same crystal plane of the palladium seeds.[51] It will allow a further discussion on Ir catalyzed reactions, both in liquid and vapor phase. As an experimental research this is, a computational chemistry study could be further applied to this research. With simulation by Density Function Theory (DFT), we will have a better understanding on how this mechanism evolved, and if this phenomena will happen on other metal surface, in an economic and effective way.

REFERENCES

1. Sorrell, S., et al., *Shaping the global oil peak: A review of the evidence on field sizes, reserve growth, decline rates and depletion rates.* Energy, 2012. **37**(1): p. 709-724.

2. Sovacool, B.K. and M.A. Brown, *Energy and American society-thirteen myths*. 2007: Springer.

3. Bezdek, R., R. Hirsch, and R. Wendling, *Peaking of World Oil Production: impacts, mitigation and risk management.* Prepared for the United States Department of Energy, 2005.

4. Hubbert, M.K. and W.W. Rubey, *Role of fluid pressure in mechanics of overthrust faulting I. Mechanics of fluid-filled porous solids and its application to overthrust faulting.* Geological Society of America Bulletin, 1959. **70**(2): p. 115-166.

5. Berndes, G., M. Hoogwijk, and R. van den Broek, *The contribution of biomass in the future global energy supply: a review of 17 studies.* Biomass and bioenergy, 2003. **25**(1): p. 1-28.

6. Besson, M., P. Gallezot, and C. Pinel, *Conversion of Biomass into Chemicals over Metal Catalysts.* Chemical Reviews, 2014. **114**(3): p. 1827-1870.

7. SUEZ, G. and A. Vattenfall, *Forest Sustainability and Carbon Balance of EU Importation of North American Forest Biomass for Bioenergy Production.* 2013.

8. Caputo, A.C., et al., *Economics of biomass energy utilization in combustion and gasification plants: effects of logistic variables.* Biomass and Bioenergy, 2005. **28**(1): p. 35-51.

9. Huber, G.W., S. Iborra, and A. Corma, *Synthesis of Transportation Fuels from Biomass: Chemistry, Catalysts, and Engineering.* Chemical Reviews, 2006. **106**(9): p. 4044-4098.

10. Gallezot, P., *Conversion of biomass to selected chemical products.* Chemical Society Reviews, 2012. **41**(4): p. 1538-1558.

11. Corma, A., S. Iborra, and A. Velty, *Chemical Routes for the Transformation of Biomass into Chemicals.* Chemical Reviews, 2007. **107**(6): p. 2411-2502.

12.   Chheda, J.N., G.W. Huber, and J.A. Dumesic, *Liquid-Phase Catalytic Processing of Biomass-Derived Oxygenated Hydrocarbons to Fuels and Chemicals.* Angewandte Chemie International Edition, 2007. **46**(38): p. 7164-7183.

13.   Chheda, J.N., Y. Roman-Leshkov, and J.A. Dumesic, *Production of 5-hydroxymethylfurfural and furfural by dehydration of biomass-derived mono- and poly-saccharides.* Green Chemistry, 2007. **9**(4): p. 342-350.

14.   Dutta, S., et al., *Direct conversion of cellulose and lignocellulosic biomass into chemicals and biofuel with metal chloride catalysts.* Journal of Catalysis, 2012. **288**: p. 8-15.

15.   Azadi, P., et al., *Liquid fuels, hydrogen and chemicals from lignin: A critical review.* Renewable and Sustainable Energy Reviews, 2013. **21**: p. 506-523.

16.   Holladay, J., T. Werpy, and D. Muzatko, *Catalytic Hydrogenation of Glutamic Acid*, in *Proceedings of the Twenty-Fifth Symposium on Biotechnology for Fuels and Chemicals Held May 4–7, 2003, in Breckenridge, CO*, M. Finkelstein, et al., Editors. 2004, Humana Press. p. 857-869.

17.   Zeitsch, K., *The chemistry and technology of furfural and its many by-products. 2000.* Elsevier Science BV.

18.   Zheng, H.-Y., et al., *Towards understanding the reaction pathway in vapour phase hydrogenation of furfural to 2-methylfuran.* Journal of Molecular Catalysis A: Chemical, 2006. **246**(1–2): p. 18-23.

19.   Nagaraja, B.M., et al., *Vapor phase selective hydrogenation of furfural to furfuryl alcohol over Cu–MgO coprecipitated catalysts.* Journal of Molecular Catalysis A: Chemical, 2007. **265**(1–2): p. 90-97.

20.   Sharma, R.V., et al., *Liquid phase chemo-selective catalytic hydrogenation of furfural to furfuryl alcohol.* Applied Catalysis A: General, 2013. **454**(0): p. 127-136.

21.   Thomas, J.M., W.J. Thomas, and H. Salzberg, *Introduction to the principles of heterogeneous catalysis.* Journal of The Electrochemical Society, 1967. **114**(11): p. 279C-279C.

22.   Bond, G.C., *Catalysis by metals.* 1962: Academic Press.

23.   Blaser, H.U., et al., *Selective hydrogenation for fine chemicals: recent trends and new developments.* Advanced Synthesis & Catalysis, 2003. **345**(1-2): p. 103-151.

24.   Heitbaum, M., F. Glorius, and I. Escher, *Asymmetric heterogeneous catalysis.* Angewandte Chemie International Edition, 2006. **45**(29): p. 4732-4762.

25.   Arakawa, H., et al., *Catalysis research of relevance to carbon management: progress, challenges, and opportunities.* Chemical Reviews, 2001. **101**(4): p. 953-996.

26.   Zaera, F., *Shape-Controlled Nanostructures in Heterogeneous Catalysis.* ChemSusChem, 2013. **6**(10): p. 1797-1820.

27.   Zaera, F., *Nanostructured materials for applications in heterogeneous catalysis.* Chemical Society Reviews, 2013. **42**(7): p. 2746-2762.

28.   Shiju, N.R. and V.V. Guliants, *Recent developments in catalysis using nanostructured materials.* Applied Catalysis A: General, 2009. **356**(1): p. 1-17.

29.   Nørskov, J.K., et al., *The nature of the active site in heterogeneous metal catalysis.* Chemical Society Reviews, 2008. **37**(10): p. 2163-2171.

30.   Zaera, F., *The new materials science of catalysis: Toward controlling selectivity by designing the structure of the active site.* The Journal of Physical Chemistry Letters, 2010. **1**(3): p. 621-627.

31.   Lim, B., et al., *Shape-Controlled Synthesis of Pd Nanocrystals in Aqueous Solutions.* Advanced Functional Materials, 2009. **19**(2): p. 189-200.

32.   Crespo-Quesada, M., et al., *Size and Shape-controlled Pd Nanocrystals on ZnO and SiO2: When the Nature of the Support Determines the Active Phase.* Chemcatchem, 2014. **6**(3): p. 767-771.

33.   Jin, M., et al., *Palladium nanocrystals enclosed by {100} and {111} facets in controlled proportions and their catalytic activities for formic acid oxidation.* Energy & Environmental Science, 2012. **5**(4): p. 6352-6357.

34.   Pushkarev, V.V., et al., *High Structure Sensitivity of Vapor-Phase Furfural Decarbonylation/Hydrogenation Reaction Network as a Function of Size and Shape of Pt Nanoparticles.* Nano Letters, 2012. **12**(10): p. 5196-5201.

35.   Nakagawa, Y., M. Tamura, and K. Tomishige, *Catalytic Reduction of Biomass-Derived Furanic Compounds with Hydrogen*, in *Acs Catalysis*. 2013. p. 2655-2668.

36.   Yan, K., et al., *Production, properties and catalytic hydrogenation of furfural to fuel additives and value-added chemicals.* Renewable & Sustainable Energy Reviews, 2014. **38**: p. 663-676.

37.   Gilkey, M.J., et al., *Mechanistic Insights into Metal Lewis Acid-Mediated Catalytic Transfer Hydrogenation of Furfural to 2-Methylfuran.* ACS Catalysis, 2015. **5**(7): p. 3988-3994.

38.   Panagiotopoulou, P. and D.G. Vlachos, *Liquid phase catalytic transfer hydrogenation of furfural over a Ru/C catalyst.* Applied Catalysis A: General, 2014. **480**: p. 17-24.

39.   Jae, J., et al., *The Role of Ru and RuO2 in the Catalytic Transfer Hydrogenation of 5-Hydroxymethylfurfural for the Production of 2,5-Dimethylfuran.* ChemCatChem, 2014. **6**(3): p. 848-856.

40.   Wojcik, B.H., *Catalytic Hydrogenation of Furan Compounds.* Industrial & Engineering Chemistry, 1948. **40**(2): p. 210-216.

41.   Hronec, M. and K. Fulajtarová, *Selective transformation of furfural to cyclopentanone.* Catalysis Communications, 2012. **24**: p. 100-104.

42.   Nakagawa, Y., et al., *Total Hydrogenation of Furfural and 5-Hydroxymethylfurfural over Supported Pd–Ir Alloy Catalyst.* ACS Catalysis, 2014. **4**(8): p. 2718-2726.

43.   Yu, W., et al., *One-step hydrogenation–esterification of furfural and acetic acid over bifunctional Pd catalysts for bio-oil upgrading.* Bioresource Technology, 2011. **102**(17): p. 8241-8246.

44.   Reyes, P., et al., *Selective hydrogenation of furfural on Ir/TiO2 catalysts.* Química Nova, 2010. **33**(4): p. 777-780.

45.   Tamura, M., et al., *Rapid synthesis of unsaturated alcohols under mild conditions by highly selective hydrogenation.* Chemical Communications, 2013. **49**(63): p. 7034-7036.

46. Seo, G. and H. Chon, *Hydrogenation of furfural over copper-containing catalysts.* Journal of Catalysis, 1981. **67**(2): p. 424-429.

47. Li, H., et al., *Liquid phase hydrogenation of furfural to furfuryl alcohol over the Fe-promoted Ni-B amorphous alloy catalysts.* Journal of molecular catalysis A: Chemical, 2003. **203**(1): p. 267-275.

48. Ordomsky, V.V., et al., *Biphasic single-reactor process for dehydration of xylose and hydrogenation of produced furfural.* Applied Catalysis A: General, 2013. **451**: p. 6-13.

49. Gorlov, Y.I., M.M. Konoplya, and A.A. Chuiko, *Mechanism for the dehydration and rehydration of silica.* Theoretical and Experimental Chemistry, 1981. **16**(3): p. 263-266.

50. Du, Y., et al., *Thermal decomposition behaviors of PVP coated on platinum nanoparticles.* Journal of applied polymer science, 2006. **99**(1): p. 23-26.

51. Xia, X.H., et al., *Facile Synthesis of Iridium Nanocrystals with Well-Controlled Facets Using Seed-Mediated Growth.* Journal of the American Chemical Society, 2014. **136**(31): p. 10878-10881.